Incorporation of Transmembrane Peptides from the Vacuolar H^+-ATPase in Phospholipid Membranes: Spin-Label Electron Paramagnetic Resonance and Polarized Infrared Spectroscopy†

Zoltán Kóta,‡,§ Tibor Páli,‡,§ Neil Dixon,|| Terry P. Kee,|| Michael A. Harrison,|| John B. C. Findlay,|| Malcolm E. Finbow,⊥ and Derek Marsh*,‡

Max-Planck-Institut für biophysikalische Chemie, Abt. Spektroskopie, 37070 Göttingen, Germany, Institute of Biophysics, Biological Research Centre, 6701 Szeged, Hungary, School of Chemistry and School of Biochemistry and Molecular Biology, University of Leeds, Leeds LS2 9JT, U.K., and Department of Biological and Biomedical Sciences, Glasgow Caledonian University, Glasgow G4 0BA, U.K.

Received December 21, 2007

ABSTRACT: Peptides were designed that are based on candidate transmembrane sequences of the V_o-sector from the vacuolar H^+-ATPase of *Saccharomyces cerevisiae*. Spin-label EPR studies of lipid–protein interactions were used to characterize the state of oligomerization, and polarized IR spectroscopy was used to determine the secondary structure and orientation, of these peptides in lipid bilayer membranes. Peptides corresponding to the second and fourth transmembrane domains (TM2 and TM4) of proteolipid subunit *c* (Vma3p) and of the putative seventh transmembrane domain (TM7) of subunit *a* (Vph1p) are wholly, or predominantly, α-helical in membranes of dioleoyl phosphatidylcholine. All three peptides self-assemble into oligomers of different sizes, in which the helices are differently inclined with respect to the membrane normal. The coassembly of rotor (Vma3p TM4) and stator (Vph1p TM7) peptides, which respectively contain the glutamate and arginine residues essential to proton transport by the rotary ATPase mechanism, is demonstrated from changes in the lipid interaction stoichiometry and helix orientation. Concanamycin, a potent V-ATPase inhibitor, and a 5-(2-indolyl)-2,4-pentadienoyl inhibitor that exhibits selectivity for the osteoclast subtype, interact with the membrane-incorporated Vma3p TM4 peptide, as evidenced by changes in helix orientation; concanamycin additionally interacts with Vph1p TM7, suggesting that both stator and rotor elements contribute to the inhibitor site within the membrane. Comparison of the peptide behavior in lipid bilayers is made with membranous subunit *c* assemblies of the 16-kDa proteolipid from *Nephrops norvegicus*, which can substitute functionally for Vma3p in *S. cerevisiae*.

The vacuolar H^+-ATPases (V-ATPases[1]) are proton pumps found in the endomembranes (vacuoles, endosomes, lysosomes, and secretory vesicles) of eukaryotes, and in specialized regions of certain plasma membranes, most notably in osteoclasts (see refs *1* and *2*, for reviews). In the latter, the V-ATPase is responsible for acidification of the extracellular compartment, at the surface of the resorbing bone. Osteoporosis results from excessive bone resorption, and consequently, selective inhibition of the osteoclast V-ATPase offers a potential therapeutic strategy. The classical V-ATPase inhibitors, bafilomycin and concanamycin, target the intramembrane V_o-sector of the enzyme (*3–5*), as most probably also does the 5-(2-indolyl)-2,4-pentadienoyl family of inhibitors (*6*), which was designed on the basis of structure–activity relationships with the macrolide antibiotics (*7*) and members of which display a selectivity for the osteoclast subtype (*7, 8*).

Proton translocation by the V-ATPase is thought to occur via rotary catalysis, in which a 16-kDa *c*-type subunit (Vma3p, Vma11p, or Vma16p in yeast) of the proteolipid rotor assembly interacts with the 100-kDa subunit *a* (Vph1p in yeast) of the stator assembly (*9, 10*). Together, these two assemblies constitute the transmembrane V_o-sector of the enzyme, the stator being attached by a peripheral stalk to the catalytic V_1-sector (see Figure 1 for a schematic arrangement of the transmembrane region). A glutamate

† This work was supported by contract no. QLG-CT-2000-01801 of the European Commision and in part by the Hungarian Science Research Fund (K68804 and F67735).

* Corresponding author. Derek Marsh, Max-Planck-Institut für biophysikalische Chemie, Abt. Spektroskopie, 37070 Göttingen, Germany. Tel: +49-551 201 1285. Fax: +49-551 201 1501. E-mail: dmarsh@gwdg.de.

‡ Max-Planck-Institut für biophysikalische Chemie.

§ Biological Research Centre.

|| University of Leeds.

⊥ Glasgow Caledonian University.

[1] Abbreviations: V-ATPase, vacuolar H^+-ATPase; TM, transmembrane; INDOL0, 5-(5,6-dichloro-2-indolyl)-2-methoxy-*N*-(1,2,2,6,6-pentamethylpiperidin-4-yl)-2,4-pentadienamide; DMPG and DOPG, 1,2-dimyristoyl- and 1,2-dioleoyl-*sn*-glycero-3-phosphoglycerol; DMPC, DPPC, and DOPC, 1,2-dimyristoyl-, 1,2-dipalmitoyl-, and 1,2-dioleoyl-*sn*-glycero-3-phosphocholine; 14-SASL, 14-(4,4-dimethyloxazolidine-*N*-oxyl) stearic acid; 14-PGSL and -PCSL, 1-acyl-2-[14-(4,4-dimethyloxazolidine-*N*-oxyl)]stearoyl-*sn*-glycero-3-phosphoglycerol and -phosphocholine; HFIP, hexafluoroisopropanol; HEPES, *N*-(2-hydroxyethyl)piperazine-*N*′-2-ethanesulphonic acid; EDTA, ethylenediaminetetraacetic acid; DMSO, dimethyl sulfoxide; EPR, electron paramagnetic resonance; IR, infrared; ATR, attenuated total reflectance.

10.1021/bi7025112 CCC: $40.75 © 2008 American Chemical Society
Published on Web 02/29/2008

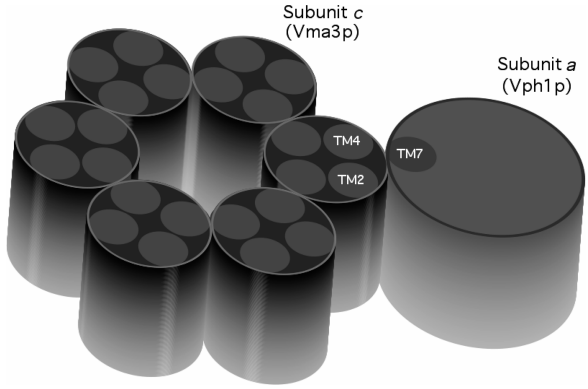

FIGURE 1: Schematic diagram of the arrangement of the V_o subunits (Vma3p and Vph1p) and putative transmembrane helices (TM) in the V-ATPase. The central hexameric arrangement of subunits *c* constitutes the rotor, and the outer 100-kDa subunit *a* represents the stator in the rotary mechanism proposed for sequential proton transport. The proton translocation pathway is thought to be at the subunit interface between TM4 and TM7.

residue in subunit *c* and an arginine residue in subunit *a* are found by mutation studies to be required for proton transport. In yeast, the essential glutamate is Glu^{137}, which is situated in the fourth putative transmembrane helix, TM4, of Vma3p (*11, 12*). The essential arginine is correspondingly Arg^{735}, situated in the seventh putative transmembrane helix, TM7, of Vph1p (*13*). A plausible transport mechanism involves the release of a proton from the carboxyl side chain of Glu^{137} by forming a salt bridge with Arg^{735} and ensuing stabilization of Glu^{137} in the ionized state, prior to picking up a further proton on rotation of the Vma3p assembly relative to the Vph1p subunit.

Currently, a high resolution structure is available neither for the V_1 ATPase sector nor for the V_o proton translocation sector of the vacuolar ATPase. A recent structure for the transmembrane sector of a related prokaryotic V-type Na^+-transporting ATPase (NtpK) reveals that the rotor assembly consists of ten 16-kDa *c*-type proteolipid subunits arranged in a ring (*14*). Each *c*-type NtpK subunit constitutes a single transmembrane 4-helix bundle, with homologous helices 1 and 3 of the tandem repeat at the inner surface of the ring and helices 2 and 4 at the outer surface (see Figure 1). For the V-type H^+-ATPase, it has been estimated that the V_o-sector contains six copies of the 16-kDa subunit *c* (*15*), which in yeast must include single copies of the *c′* and *c″* homologues in a specific ordered assembly (*16*). Electron microscopy of two-dimensional arrays formed by the homologous 16-kDa proteolipid from *Nephrops norvegicus* also suggests a 6-fold symmetry (*17*).

In the absence of a high resolution structure of the V_o-sector, we have attempted to identify transmembrane (TM) peptides suitable for incorporation in lipid model membranes, and to study the interaction with inhibitors. Here, we investigate the intramembrane assembly of these synthetic peptides, from the stoichiometry and selectivity of lipid–protein interaction determined by spin-label EPR spectroscopy (*18–20*). The peptide conformation and transmembrane alignment is also studied by polarized IR spectroscopy (*21*), in order to characterize the secondary structure, establish suitable lipid hosts, and detect mutual interactions. Particular attention is devoted to the TM-segments of Vma3p and Vph1p that contain the critical glutamate and arginine residues, respectively.

Vma3p TM2	N^{53}IVPVIMAGIIAIYGLVVSVLVAYS^{77}
Vma3p TM3	Q^{90}LGAGLSVGLSGLAAGFAIGIVGDAGVR^{117}
Vma3p TM4	R^{124}LFVGMILILIFAEVLGLYGLIVALLLN^{151}
Vph1p TM7	I^{717}HTIEFCLNCVSHTASYLRLWALSLAHAQLSSVLWTM^{753}

FIGURE 2: Amino acid sequences of synthetic TM peptides based on the Vma3p and Vph1p subunits of the vacuolar H^+-ATPase from *Saccharomyces cerevisiae*.

MATERIALS AND METHODS

Materials. Transmembrane (TM) peptides were obtained by custom synthesis from Pepceuticals Ltd. (Leicester, UK). The amino acid sequences of the various TM peptides are given in Figure 2. Phospholipids dimyristoyl phosphatidylcholine (DMPC), dipalmitoyl phosphatidylcholine (DPPC), dioleoyl phosphatidylcholine (DOPC), dimyristoyl phosphatidylglycerol (DMPG), and dioleoyl phosphatidylglycerol (DOPG) were from Avanti Polar Lipids (Alabaster, AL). Concanamycin A was obtained from Fluka (Buchs, Switzerland). The V-ATPase inhibitor INDOL0 was synthesized according to refs *7* and *22*. Spin-labeled stearic acid, 14-SASL, with the DOXYL nitroxide group on the 14-C atom, was synthesized according to Hubbell and McConnell (*23*). Spin-labeled phosphatidylcholine, 14-PCSL, was synthesized by acylation of lysophosphatidylcholine with 14-SASL, as described in Marsh and Watts (*24*). Spin-labeled phosphatidylglycerol (14-PGSL) was prepared from 14-PCSL by headgroup exchange mediated by phospholipase D (*24*). Membranes containing the 16-kDa channel proteolipid were prepared from the hepatopancreas of the decapod *Nephrops norvegicus* by extraction with *N*-lauryl sarcosine, according to the procedures in refs *25–27*.

EPR Spectroscopy. EPR spectra were recorded on a Bruker (Rheinstetten, Germany) EMX 9-GHz spectrometer with rectangular cavity and nitrogen gas-flow temperature regulation. Samples were accommodated in 1-mm diameter glass capillaries, which were placed in a standard quartz EPR tube that contained light silicone oil for thermal stability. A solution of TM peptide plus phospholipid and 1 mol% spin label (2 mg of lipid at 7 mg/mL) in hexafluoroisopropanol (HFIP) was dried down under nitrogen and then incubated under vacuum overnight. The dry sample was hydrated with excess buffer (70 μL of 20 mM HEPES, 10 mM EDTA, pH 7.8) by vortex mixing above the chain-melting temperature of the lipid. This was then pelleted in the glass capillary by using a benchtop centrifuge. Excess supernatant was removed and the capillary was sealed.

Analysis of the two-component EPR spectra was performed by spectral addition, using least-squares optimization. In the final stage of minimization, the only free fitting parameters were the populations of the two components, and the fit was restricted to the low-field ($m_I = +1$) hyperfine manifold, which is the spectral region most sensitive to the presence of motionally restricted lipids. Single-component spectra were taken from a spectral library obtained with spin-labeled small unilamellar vesicles of dimyristoyl phosphatidylcholine for the motionally restricted component (*28*) and

with dispersions of DOPC alone for the fluid component. Fitting of EPR (and IR) spectra was performed in IGOR (Wave Metrics, Lake Oswego), using self-written code.

ATR Spectroscopy. Polarized ATR infrared spectra were recorded on a Bruker (Karlsruhe, Germany) IFS-25 Fourier transform spectrometer at a nominal resolution of 2 cm^{-1}. A horizontal ATR accessory from Specac (Orpington, U.K.) was used with a zinc selenide crystal (45° angle of incidence, 6 reflections). This was modified to seal the sample chamber hermetically from above and to thermostat the cell housing with internally circulating water from a temperature-controlled bath (Haake, Karlsruhe, Germany). The surface of the ATR crystal available for coating by the sample was 8 × 45 mm. A germanium-mounted, wire-grid, linear polarizer (Specac, Orpington, U.K) was used in the incident beam. Typically, 512 interferograms were coadded, and Fourier-transformed after two levels of zero-filling and apodization with a Blackman-Harris 3-term function.

Samples containing 40–90 μg of peptide with lipid at the desired peptide/lipid mole ratio were dried down on the ZnSe ATR crystal from solution in HFIP. Spectra of the dry sample were then recorded at the desired temperatures with radiation polarized parallel and perpendicular to the plane of incidence. The sample was then hydrated with 30 μL of a D_2O-based buffer (10 mM HEPES, pH 7.8) by incubating above the chain-melting transition of the lipid bilayer, prior to recording again the polarized ATR spectra. After baseline subtraction, bands in the amide I, II, and ester CO region (1520–1750 cm^{-1}), and in the CH stretching region (2830–2975 cm^{-1}), were fitted with Lorentzian components by using nonlinear least-squares minimization. Second-derivative spectra were used to provide initial estimates of the component band positions. Dichroic ratios were calculated by using the integrated intensities of the α-helical bands in the 1655 cm^{-1} region and those of the CH symmetric stretching bands in the region of 2850 cm^{-1}.

Helix and lipid-chain order parameters are calculated from the measured dichroic ratios, $R(\Theta)$, according to ref *21*:

$$\langle P_2(\cos\gamma)\rangle = \frac{E_x^2/E_y^2 - R(\Theta) + E_z^2/E_y^2}{P_2(\cos\Theta)\left[E_x^2/E_y^2 - R(\Theta) - 2E_z^2/E_y^2\right]} \quad (1)$$

where γ is the orientation of the molecular axis relative to the normal to the orienting substrate (i.e., the ATR plate), and Θ is the orientation of the transition moment relative to the molecular axis. For the amide I band of an α-helix, $\Theta = 38°$ (*29, 30*), and for the CH stretching bands of a lipid chain, $\Theta = 90°$. The strengths of the electric field components, with a zinc selenide ATR crystal, are $E_x^2/E_y^2 = 0.450$ and $E_z^2/E_y^2 = 1.550$ in the thick film approximation, which is appropriate to the amount of material used (*21*). Order parameters are related to the molecular tilt angle by

$$\langle P_2(\cos\gamma)\rangle = \frac{1}{2}(3\langle\cos^2\gamma\rangle - 1) \quad (2)$$

where angular brackets indicate summation over the (normalized) orientational distribution in γ. These order parameters are a composite of the molecular orientation in the membrane and the degree of alignment of the membrane relative to the surface of the ATR crystal. Effective tilt angles, γ_{eff}, are obtained from $\langle\cos^2\gamma\rangle$ by assuming a singular value of γ. Values of γ_{eff} obtained for the lipid chains in the gel phase are used to assess the degree of macroscopic alignment of the membranes, as described in the Results section.

To obtain the true absorbed intensity that reflects relative populations in aligned samples, it is necessary to combine absorbances, $A_{//}$ and $A_{\perp}$, for parallel and perpendicular polarized radiation (*31*). The appropriate admixture of $A_{\perp}$with $A_{//}$ that allows quantitatively for the spectral dichroism is $A_{//} + (2E_z^2/E_y^2 - E_x^2/E_y^2)A_{\perp}$, in the present geometry. The fractional population of a particular component *j* is, therefore, given by

$$f_j = \frac{A_{//,j} + \left(2\frac{E_z^2}{E_y^2} - \frac{E_x^2}{E_y^2}\right)A_{\perp,j}}{\sum_j \left(A_{//,j} + \left(2\frac{E_z^2}{E_y^2} - \frac{E_x^2}{E_y^2}\right)A_{\perp,j}\right)} \quad (3)$$

where $A_{//j}$ and $A_{\perp,j}$ are the integrated absorbances of component *j* that are obtained from band fitting to the parallel and perpendicularly polarized spectra, respectively.

Thermodynamic Calculations. Free energies of transfer, hydropathy profiles, and hydrophobic moments are calculated according to the whole-residue scale for transfer from octanol to water, and the octanol-minus-interface scale, of Wimley and White (*32*). Calculations are implemented using the Membrane Protein Explorer package (MPEx) of Jayasinghe et al. (*33*). Hydrophobic moments are defined according to ref *34*. Amino acid sequences were taken from the PIR Database; accession codes: PXBYL6, A42970, and S32544, for Vma3p, Vph1p, and 16-kDa, respectively (*35*).

RESULTS

Vma3p Proteolipid Hydropathy. The hydropathy profile of the vacuolar ATPase Vma3p proteolipid subunit from *Saccharomyces cerevisiae* calculated according to the octanol whole-residue free energy scale of Wimley and White (*32*) is given in the upper panel of Figure 3. Data are also given for the hydropathy profile calculated using the octanol-minus-interface scale that represents the free energy of transfer from the octanol core to a location in the membrane−water interfacial region. The lower panel of Figure 3 gives corresponding hydropathy profiles for the 16-kDa proteolipid from the hepatopancreas of *Nephrops norvegicus*, which shows 68% sequence identity with the yeast proteolipid. Four transmembrane segments are predicted on the octanol scale, of which the first in each tandem repeat is considerably less hydrophobic than the second. TM1 shows little preference for the hydrophobic core relative to the membrane interface, and TM3 energetically favors the latter location (see Table 1). These are potentially characteristics of interior or pore-lining transmembrane segments (cf. Figure 1). TM4, which contains the DCCD-reactive residue Glu^{137} (Glu^{140} in *N. norvegicus*), has the largest hydrophobicity on the octanol scale, but is comparable to TM2 on the octanol-minus-interface scale. The values in Table 1 give the transfer free energies for TM4 with the Glu^{137} (or Glu^{140}) side chain negatively charged. For the protonated glutamate, these values are increased by 3.52 kcal/mol on the octanol scale or by 1.49 kcal/mol on the octanol-minus-interface scale.

Vph1p Hydropathy. Figure 4 gives hydropathy profiles for the vacuolar ATPase Vph1p stator subunit from *Saccharo-*

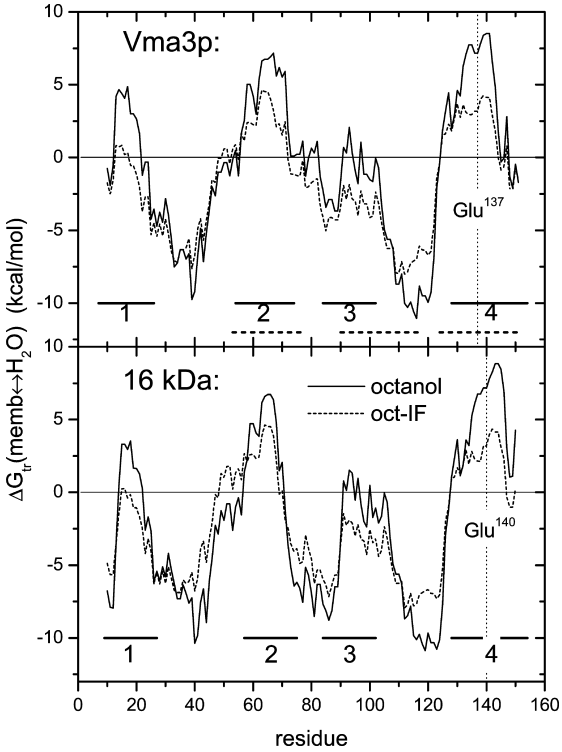

FIGURE 3: Hydropathy profile for the Vma3p proteolipid of the vacuolar ATPase from *S. cerevisiae* (upper panel) and of the 16-kDa proteolipid from *N. norvegicus* (lower panel), calculated with the whole-residue octanol partitioning scale (solid lines) of Wimley and White (*32*) and with the corresponding octanol-minus-interface scale (dashed line). Plotted is the free energy of transfer from the membrane hydrophobic core to water (solid line) or to the interfacial region of the membrane (dashed line) by using a 19-residue window. Thick horizontal lines represent energetically favourable transmembrane segments (1–4) predicted by the octanol scale. The position of the DCCD-reactive glutamate (Glu^{137}/Glu^{140}) in TM4 is indicated. Dashed horizontal lines indicate the sequence positions of the synthetic peptides.

Table 1: Hydrophobicities (i.e., Free Energy of Transfer from Membrane to Water), ΔG_{tr}, and Hydrophobic Moments, μ_H, of the Vma3p Proteolipid from *Saccharomyces cerevisiae* and the 16-kDa Proteolipid from *Nephrops norvegicus*, Predicted According to the Whole-Residue Octanol and Octanol-Minus-Interface Scales of Wimley and White (*32*)

			ΔG_{tr} (kcal/mol)		μ_H
TM segment	sequence no.	N_{res}	oct-H_2O	oct-IF	(oct-H_2O)
		S. cerevisiae			
1	7–26	20	5.32	0.88	7.65
2	54–74	21	8.34	5.86	7.02
3	84–102	19	2.06	−1.85	8.47
4	125–150	26	13.83	6.72	5.69
		N. norvegicus:			
1	9–27	19	3.53	−0.14	7.23
2	57–75	19	6.72	4.52	5.63
3	84–102	19	1.53	−1.88	5.91
4	128–154	27	13.87	5.69	6.23

myces cerevisiae. The octanol scale predicts eight transmembrane segments of 19 residues or more that have net $\Delta G_{tr} > 0$ for transfer from octanol to water. One of these, TM5, is immediately flanked by charged residues and therefore may be considered marginal. Most other putative transmembrane segments have approximately twice the transfer free energy of TM5 (see Table 2). An even number of transmembrane segments is consistent with a cytoplasmic

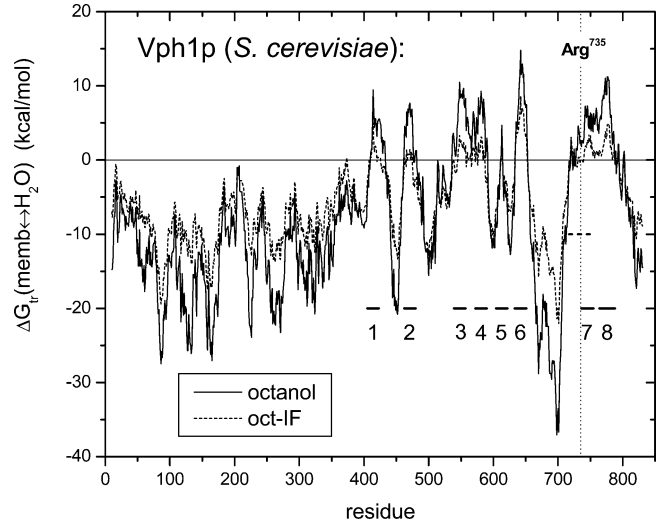

FIGURE 4: Hydropathy profile for the Vph1p subunit from vacuolar membranes of *S. cerevisiae*, calculated with the whole-residue octanol partitioning scale (solid lines) of Wimley and White (*32*) and with the corresponding octanol-minus-interface scale (dashed line). Plotted is the free energy of transfer from the membrane hydrophobic core to water (solid line) or to the interfacial region of the membrane (dashed line) by using a 19-residue window. Thick horizontal lines represent energetically favourable transmembrane segments (1–8) predicted by the octanol scale. Dashed horizontal line indicates the position of the Arg^{735} homology region, residues 717–753 of Vph1p.

Table 2: Hydrophobicities (i.e., Free Energy of Transfer from Membrane to Water), ΔG_{tr}, and Hydrophobic Moments, μ_H, of the Putative Transmembrane Segments of Vph1p from *Saccharomyces cerevisiae* Predicted According to the Whole-Residue Octanol and Octanol-Minus-Interface Scales Of Wimley and White (*32*)

			ΔG_{tr} (kcal/mol)		μ_H
TM segment	sequence no.	N_{res}	oct-H_2O	oct-IF	(oct-H_2O)
1	405–423	19	9.47	5.02	4.29
2	462–480	19	7.67	1.42	8.61
3	539–557	19	10.49	3.34	6.86
4	572–590	19	9.28	3.13	5.40
5	604–622	19	4.66	2.86	5.67
6	633–651	19	14.79	8.59	3.11
7	736–755	20	8.42	3.38	2.98
8	764–788	25	14.61	6.39	3.15

location of the C-terminus of Vph1p (*36*), as for the N-terminus (*37*).

Putative transmembrane segment TM6 is particularly hydrophobic and has a low hydrophobic moment. The TM6 segment also has a strong preference for location in the hydrophobic core, rather than the membrane interface, as is seen from the octanol-minus-interface scale. All putative TM segments identified with the octanol scale are predicted to be energetically more favorable in the hydrophobic core than at the membrane interface. For TM2, however, this difference is only marginal.

The putative transmembrane segments TM7 and TM8 also have relatively low hydrophobic moments and, in the case of TM8, also high hydrophobicity. These segments are, however, somewhat longer than the other predicted transmembrane sequences. On the octanol scale, the center position of TM7 is somewhat diffuse, but clearly is peaked on the octanol-minus-interface scale.

The highly conserved and functionally essential arginine residue Arg^{735} is immediately adjacent to the *N*-terminal of

Table 3: Hydrophobicities (i.e., Free Energy of Transfer from Membrane to Water), ΔG_{tr}, and Hydrophobic Moments, μ_H, of *Saccharomyces cerevisiae* Synthetic TM Peptides, Predicted According to the Whole-Residue Octanol and Octanol-Minus-Interface Scales of Wimley and White (*32*)

			ΔG_{tr} (kcal/mol)[a]		μ_H	
peptide	sequence no.	N_{res}	Oct-H_2O	oct-IF	oct	IF
Vma3p TM2	53–77	25	7.24 (−1.32)	4.54 (−3.48)	8.63	3.73
Vma3p TM3	90–117	28	−8.51 (−17.07)	−8.48 (−16.50)	3.26	2.21
Vma3p TM4	124–151	28	11.17 (2.61)	5.29 (−2.73)	4.86	2.09
Vph1p TM7	717–753	37	6.78 (−1.78)	1.99 (−6.03)	5.29	5.99

[a] Values in parentheses are for charged N- and C-termini.

the putative TM7 segment (c.f. *13*). A 19-residue sequence centered on Arg^{735} would have equally favorable partitioning to the membrane interface ($\Delta G_{tr} = 2.8$ kcal/mol) as to the octanol-like core ($\Delta G_{tr} = 2.6$ kcal/mol) (see Figure 4). In isolation, therefore, this segment is not expected necessarily to be transmembrane. Octanol partitioning predicted for the segment centered on Arg^{735} is much smaller than that for TM7, which is centered on residues Gln^{745}−Leu^{746}. The whole $N_r = 37$ amino acid stretch, constituting residues 717–753, has $\Delta G_{tr} = 6.78$ kcal/mol on the octanol scale and $\Delta G_{tr} = 4.79$ kcal/mol on the interfacial scale. The octanol value for this longer stretch is still less than that for the shorter 20-residue TM7 (736–755) segment, although it encompasses most of it.

Hydropathy of Synthetic TM Peptides. The synthetic TM peptides listed in Figure 2 were designed partly on the basis of the above hydropathy analysis, but based also on previous studies with site-specific labeling and cross-linking (*38–40*), on identification of flanking residues likely to provide anchoring at the membrane−water interface, and on considerations of functionality (*13, 41*). The synthetic peptides Vma3p TM2 and TM4 correspond closely to the transmembrane segments identified by hydropathy. Synthetic peptide Vma3p TM3 differs somewhat in its length and center, relative to that tentatively identified from the rather low peak in hydropathy. Synthetic peptide Vph1p TM7 is extended on the N-terminal side, relative to the transmembrane domain suggested by hydropathy analysis, to take account of the functionally important arginine Arg^{735}, as discussed above. Throughout, the synthetic peptides used in this study are distinguished from TM segments proposed solely on hydropathy considerations by prefixing the name of the protein (Vma3p or Vph1p) from which the peptide sequence is taken.

Table 3 gives the hydrophobic free energies of transfer (and hydrophobic moments) for the various synthetic peptides used in this study. Apart from any differences in sequence position and length, these data differ also from those given for putative transmembrane segments in Tables 1 and 2 in that the N-terminal amine and C-terminal carboxyl groups are included. Two sets of values are given, for neutral and for charged N- and C-termini, respectively. The peptides all include a polar residue at the N- and C-termini. With the exception of Vma3p TM3, all are predicted to be embedded in the membrane, if the terminal amine and carboxyl groups are uncharged. Vma3p TM3 is predicted to partition preferentially into water, rather than having a membrane location. This prediction, however, takes no account of the nonuniform distribution of polar residues and the possibility of membrane partitioning as a bitopic amphiphile.

Spin-Labeled Phosphatidylcholine and Vma3p TM4 in DOPC. Figure 5 shows the EPR spectra of the 14-PCSL phosphatidylcholine spin label in bilayer membranes of dioleoyl phosphatidylcholine containing the peptide at a relatively high peptide/lipid ratio of 1:12 mol/mol. Spectra are shown for various temperatures in the fluid phase of DOPC bilayers. (The chain-melting temperature for DOPC is −21 °C.) The spectra all consist of two components: that with larger hyperfine splitting, which is visible in the outer wings of the spectrum, corresponds to spin-labeled lipids interacting directly with the intramembranous section of the peptide assemblies, and that with smaller hyperfine splitting, which gives rise to the three sharper lines in the center of the spectrum, corresponds to spin-labeled lipids in the fluid bilayer regions of the membrane. Rotational diffusion of the motionally restricted lipids lies in the slow-motion regime of spin-label EPR spectroscopy. The line shape of the fluid component, therefore, narrows much more rapidly with increasing temperature than does that of the motionally restricted component and becomes much more dominant (in terms of lineheight) relative to the latter at higher temperatures.

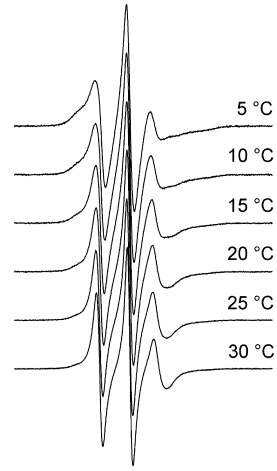

FIGURE 5: Temperature dependence of the EPR spectra from the 14-PCSL spin-labeled phosphatidylcholine in bilayer membranes of dioleoyl phosphatidylcholine (DOPC) containing the Vma3p TM4 peptide at a lipid/peptide ratio of 12:1 mol/mol. Total scan width = 120 G.

Assignment of the motionally restricted component (which is absent from spectra of fluid DOPC alone) to lipids associated directly with the transmembrane section of the peptide comes from comparison with similar experiments on integral membrane proteins (*19*). Quantitation of the relative population of motionally restricted lipid, by spectral addition/subtraction, reveals that 31 ± 2% of the lipids are motionally restricted over the range 5 to 25 °C. This translates to approximately $N_b = 4$ motionally restricted lipids per Vma3p TM4 peptide monomer. Such a relatively low lipid/protein stoichiometry implies that the peptides are assembled into oligomeric aggregates in the lipid membranes, and thus, not all intramembranous surfaces of the peptide

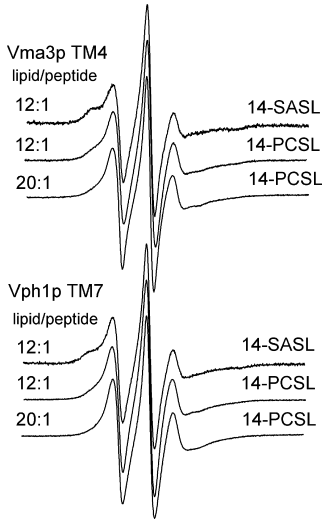

FIGURE 6: EPR spectra from the 14-SASL stearic acid and 14-PCSL phosphatidylcholine spin labels in DOPC bilayer membranes containing the Vma3p TM4 or Vph1p TM7 peptide at lipid/peptide ratios of 20:1 and 12:1 mol/mol, as indicated. $T = 10$ °C; total scan width = 120 G.

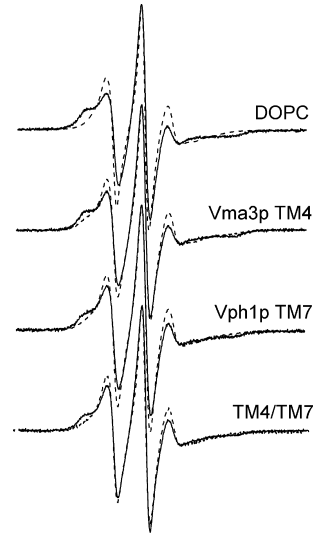

FIGURE 7: EPR spectra from the 14-PCSL phosphatidylcholine spin label in DOPC bilayer membranes, with and without the Vma3p TM4 or Vph1p TM7 peptide or their 1:1 mol/mol mixture, at a lipid/peptide ratio 12:1 mol/mol. Spectra are shown for samples in the presence (solid line) and in the absence (dotted line) of concanamycin A at a 1:1 mole ratio with respect to lipid. $T = 10$ °C; total scan width = 120 G.

are exposed to lipid (*42*). As will be seen later, the Vma3p TM4 peptides are in a predominantly α-helical conformation at this lipid/peptide ratio in DOPC.

Spin-Labeled Lipids and TM Peptides in DOPC. Figure 6 shows the EPR spectra of spin-labeled stearic acid (14-SASL) and of spin-labeled phosphatidylcholine (14-PCSL) in DOPC membranes containing either the Vma3p TM4 or the Vph1p TM7 peptide. As will be seen later, the peptides again are predominantly α-helical under these conditions. The spectra of 14-PCSL in membranes containing the Vph1p TM7 peptide at 1:12 mol/mol peptide/lipid ratio also reveal two components, but the motionally restricted component is less evident than in membranes containing the Vma3p TM4 peptide. This indicates that the degree of oligomerization is greater for the Vph1p TM7 peptide than for the Vma3p TM4 peptide because the fraction of peptide surface exposed to lipid is smaller. The motionally restricted component is much reduced in 1:20 mol/mol Vma3p TM4/DOPC membranes, and in Vph1p TM7/DOPC membranes, it is no longer visible at this lower peptide/lipid ratio. In membranes containing either peptide, the population of motionally restricted 14-SASL is greater than that for 14-PCSL. This indicates a preferential association of stearic acid with the peptide assemblies, compared with phosphatidylcholine.

Quantitation of the two-component spectra in Figure 6 by spectral subtraction/addition and spectral integration reveals that 48% of 14-SASL and 33% of 14-PCSL are motionally restricted by Vma3p TM4 at a lipid/protein ratio of 12:1 mol/mol. Correspondingly, 35% of 14-SASL and 23% of 14-PCSL are motionally restricted by Vph1p TM7 at the same lipid/protein molar ratio.

Similar experiments were also performed with an equimolar mixture of the Vma3p TM4 and Vph1p TM7 peptides in DOPC membranes (see Figure 7, below). The spectrum of spin-labeled phosphatidylcholine (14-PCSL) from membranes containing the 1:1 mol/mol peptide mixture is rather similar to that from DOPC containing the Vph1p TM7 peptide alone, at the same total peptide/lipid ratio (ca. 18% motionally restricted). It evidences none of the larger population of motionally restricted lipids characteristic of lipid–protein interaction with the Vma3p TM4 peptide (cf. Figure 6). This indicates coassembly of the two complementary peptides from the Vma3p and Vph1p subunits, in oligomers that presumably are closer in size to those of the Vph1p TM7 peptide alone than those of the Vma3p TM4 peptide. For slightly different reasons, this also implies that the affinity for association between Vma3p TM4 and Vph1p TM7 is greater than that for the self-association of either peptide. In contrast to the results with 14-PCSL, the spectrum of 14-SASL from membranes containing the 1:1 mol/mol peptide mixture is more similar to that from DOPC containing the Vma3p TM4 peptide alone, at the same total peptide/lipid ratio (ca. 46% motionally restricted). The selectivity for fatty acids, therefore, appears to be higher than that for assemblies of the Vph1p TM7 peptide alone, in spite of the fact that the oligomer size is larger.

Inhibitors, Spin-Labeled Lipids and TM Peptides in DOPC. Figure 7 shows the EPR spectra of 14-PCSL in DOPC membranes containing the Vma3p TM4 peptide or the Vph1p TM7 peptide, or a 1:1 mol/mol mixture of both peptides, in the presence and absence of concanamycin A. An equimolar amount of inhibitor relative to lipid was used. Control spectra for DOPC membranes without peptide are also included in Figure 7 (uppermost spectra). In each case, addition of concanamycin A to the membrane results in an increase in the motionally restricted lipid component. This effect is, however, an intrinsic property of the interaction of concanamycin with lipids because a motionally restricted component is induced in DOPC membranes alone at this rather high inhibitor/lipid ratio. An indirect effect possibly of this type has been observed previously in spin-labeled *Nephrops* 16-kDa membranes and in yeast vacuolar membranes, via the influence of concanamycin A on the overall rotational diffusion of the spin-labeled protein (*6*). Recent EPR studies with spin-labeled hydrophobic V-ATPase inhibitors in 16-kDa and vacuolar membranes have also shown enhancement of the motionally restricted population at high concentrations of concanamycin (*8*).

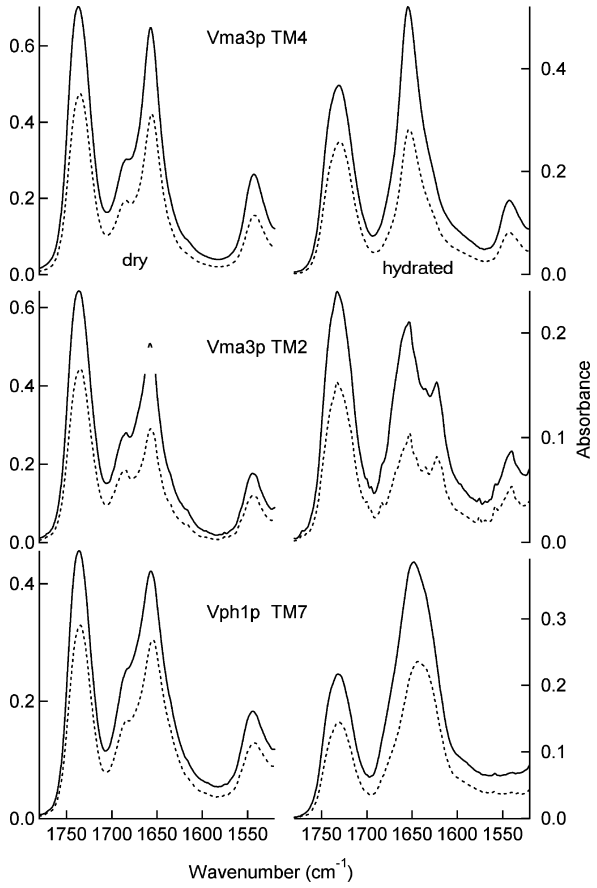

FIGURE 8: Amide region in the polarized ATR infrared spectra of Vma3p TM4 (top), Vma3p TM2 (middle), and Vph1p TM7 (bottom) peptides in aligned DOPC multibilayers, at a lipid/peptide ratio of 20:1 mol/mol. Left column, in the dry state and right column, in the fully hydrated state (in D_2O buffer) at a temperature of 36 °C. Solid lines are for parallel-polarized (0°) radiation; dotted lines are for perpendicular-polarized (90°) radiation.

Polarized IR of TM Peptides in DOPC. Figure 8 shows the amide region in the polarized ATR spectra of the Vma3p TM4, Vma3p TM2, and Vph1p TM7 peptides in DOPC at a lipid/peptide ratio of 20:1 mol/mol. Spectra are presented for both dry and fully hydrated aligned membranes. A pronounced dichroism is evident in all cases. In the dry state, the amide I region is dominated by a sharp band at the α-helical frequency of ca. 1655 cm^{-1}, for all samples. Upon hydration, in the fluid membrane phase, the amide I band broadens, and varying amounts of intensity appear in the low frequency region at ca. 1630 cm^{-1} that is characteristic of β-sheet components. For the Vma3p TM4 peptide, this latter component is very minor and unresolved; for the Vph1p TM7 peptide, this component is evident as an asymmetric shoulder; for the Vma3p TM2 peptide, it appears as a resolved peak. In all cases, the majority species is α-helical.

The dichroic ratios of the amide I α-helical component were determined by band fitting (see later, below). Table 4 gives values of the helix order parameter, $\langle P_2(\cos\gamma)\rangle$, deduced from eq 1, and for the effective tilt that is obtained from eq 2 by assuming a fixed angle γ. Corresponding data for the lipid chains that are obtained from the dichroic ratios of the CH symmetric stretch band at 2850 cm^{-1} are also given in Table 4. The helix tilt is characterized by a lower order compared to that for the lipid chains for all three peptides. This is the case at temperatures of 10 and 36 °C, both in the fluid membrane phase of DOPC. Of the three peptides, Vma3p TM2 is characterized by the highest degree of order and Vph1p TM7 by the lowest order. The difference between the Vma3p TM4 and Vph1p TM7 peptides is found consistently also at a lipid/peptide ratio of 50:1 mol/mol in DOPC and is most probably attributable to the considerably greater length of the Vph1p TM7 peptide, which must extend outside the DOPC bilayer membrane.

Table 4: Order Parameters, $\langle P_2(\cos\gamma)\rangle$, and Effective Tilts, γ_{eff} (°), of the α-Helices (Amide I) of Vma3p TM4, Vma3p TM2, and Vph1p TM7 Peptides and of the Lipid Chains (CH_2) in Aligned Hydrated DOPC Multibilayers, at a Lipid/Peptide Ratio of 20:1 mol/mol and the Temperatures Indicated[a]

	CH_2		amide I	
peptide	10 °C	36 °C	10 °C	36 °C
Vma3p TM4	0.27 (44°)	0.27 (44°)	−0.09 (59°)	−0.01 (55°)
Vam3p TM2	0.31 (43°)	0.24 (46°)	0.04 (53°)	0.22 (46°)
Vph1p TM7	0.28 (44°)	0.25 (45°)	−0.25 (66°)	−0.14 (61°)

[a] Order parameters and effective tilts (given in parentheses) are obtained from eqs 1 and 2, respectively.

When the Vma3p TM4 and Vph1p TM7 peptides are combined at a 1:1 mole ratio in DOPC such that the total peptide/lipid ratio is 1:25 mol/mol, the average order parameters and effective tilts of the peptide helices are very similar to those of Vma3p TM4 alone in DOPC at 1:20 mole ratio. This is found at both 10 and 36 °C (data not shown) and suggests interaction between the Vma3p TM4 and Vph1p TM7 peptides such that the order of the Vph1p TM7 helix is increased by association with the Vma3p TM4 peptide. These results parallel those above from EPR, which give evidence for interaction between the Vma3p and Vph1p peptides from changes in the stoichiometry of motionally restricted lipids.

Polarized IR of the Vma3p TM4 Peptide at Different Lipid/Peptide Ratios. Figure 9 shows the amide I region in the polarized ATR infrared spectra of the Vma3p TM4 peptide in fluid hydrated DOPC membranes at different lipid/peptide ratios. The amide I spectral region is dominated by the α-helical band at ca. 1655 cm^{-1} over the complete range of lipid/peptide ratios. A minor spectral component at the β-sheet frequency of ca. 1630 cm^{-1} appears with any appreciable intensity only for the low lipid/peptide ratios of 20:1 and 12:1 mol/mol.

Table 5 presents the order parameters and effective tilts of the α-helices and the lipid chains for Vma3p TM4 in fluid hydrated DOPC at the different lipid/peptide ratios. Increasing peptide content tends to increase the order of the lipid chains somewhat, whereas the order of the peptide appears to decrease at the lowest lipid/peptide ratio. This effect is particularly evident at 10 °C but is also the case at the higher temperature.

Polarized IR of the Vma3p TM4 Peptide in Different Lipids. Table 6 presents the order parameters and effective tilts of the α-helices and the lipid chains for Vma3p TM4 in hydrated bilayer membranes of different lipid species. Data are given at temperatures of 10 and 36 °C (45 °C for DPPC), which correspond to the gel and fluid phases, respectively, for the lipids with saturated chains (DMPC, DMPG, and DPPC). In the gel phase at 10 °C, the effective tilt of the lipid chains is 30–33°, which is close to the static chain tilt found by X-ray diffraction in the $L_{\beta'}$ gel phase for saturated

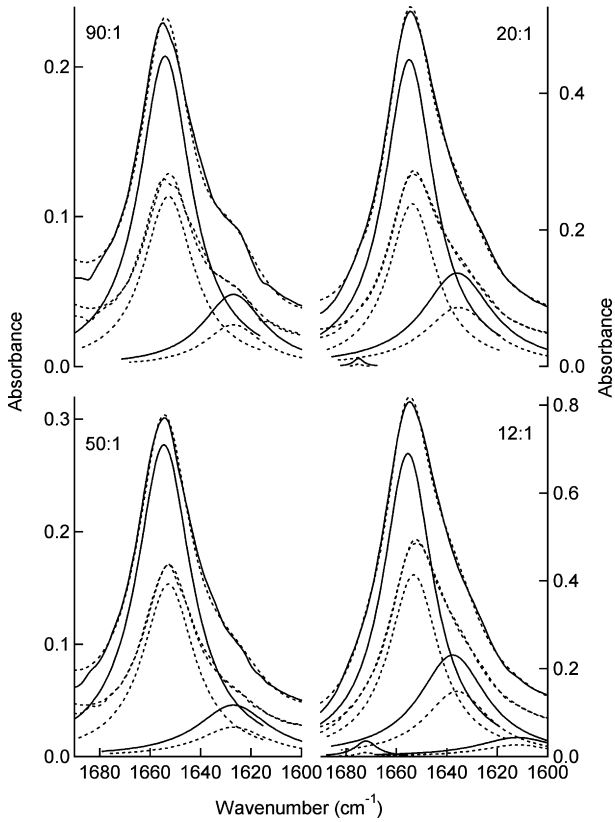

FIGURE 9: Amide I region in the polarized ATR infrared spectra of the Vma3p TM4 peptide in aligned DOPC multibilayers in D_2O buffer, at the lipid/peptide ratios indicated: 90:1 mol/mol, 50:1 mol/mol, 20:1 mol/mol and 12:1 mol/mol, and a temperature of 36 °C. Solid lines are for parallel-polarized (0°) radiation; dotted lines are for perpendicular-polarized (90°) radiation. Band fitting is shown below the experimental spectra, and the fitted envelope is given by dotted lines.

Table 5: Order Parameters, $\langle P_2(\cos\gamma)\rangle$, and Effective Tilts, γ_{eff} (°), of the α-Helices (Amide I) of Vma3p TM4 Peptide and of the Lipid Chains (CH_2) in Aligned Hydrated DOPC Multibilayers for Different Lipid/Peptide Molar Ratios and the Temperatures Indicated[a]

lipid/peptide (mol/mol)	CH_2		amide I	
	10 °C	36 °C	10 °C	36 °C
90:1	0.23 (46°)	0.21 (47°)	−0.04 (56°)	−0.06 (57°)
50:1	0.28 (44°)	0.30 (43°)	−0.09 (58°)	−0.05 (57°)
20:1	0.27 (44°)	0.27 (44°)	−0.09 (59°)	−0.01 (55°)
12:1	0.31 (43°)	0.27 (44°)	−0.30 (68°)	−0.18 (63°)

[a] Order parameters and effective tilts (given in parentheses) are obtained from eqs 1 and 2, respectively.

Table 6: Order Parameters, $\langle P_2(\cos\gamma)\rangle$, and Effective Tilts, γ_{eff} (°), of the α-Helices (Amide I) of Vma3p TM4 Peptide and of the Lipid Chains (CH_2) in Different Aligned Hydrated Lipid Multibilayers, at a Lipid/Peptide Ratio of 50:1 mol/mol and the Temperatures Indicated[a]

lipid	CH_2		amide I	
	10 °C	36 °C	10 °C	36 °C
DMPC	0.63 (30°)	0.44 (38°)	−0.01 (55°)	−0.02 (56°)
DPPC	0.55 (33°)	0.56 (33°)[b]	−0.08 (58°)	−0.09 (59°)[b]
DOPC	0.28 (44°)	0.30 (43°)	−0.09 (58°)	−0.05 (57°)
DMPG	0.60 (31°)	0.40 (39°)	0.12 (50°)	0.08 (51°)
DOPG	0.31 (43°)	0.31 (43°)	0.11 (51°)	0.08 (52°)

[a] Order parameters and effective tilts (given in parentheses) are obtained from 1 and 2, respectively. [b] For DPPC, 45 °C.

phosphatidylcholines and phosphatidylglycerol (*43*). This indicates that the membranes are reasonably well aligned on the ATR substrate. A somewhat higher effective tilt is found for the chains of the dimyristoyl phospholipids at 36 °C, relative to the dipalmitoyl lipid at 45 °C, which corresponds to the disordering of the chains within the fluid phase.

The order parameters of the Vma3p TM4 α-helix in the phosphatidylcholines with saturated chains are comparable to those in DOPC. This is particularly so for DMPC, where the hydrophobic thickness of the fluid lipid bilayer is closer to that of DOPC than is that of DPPC (*44*). In the two phosphatidylglycerol membranes, however, the ordering of the Vma3p TM4 helix is greater than that in the phosphatidylcholine membranes. This indicates a preferential interaction of the bulk anionic lipid with the Vma3p TM4 peptide. Correspondingly, the EPR results given above demonstrate a preferential interaction of the anionic spin-labeled fatty acid, relative to the zwitterionic phosphatidylcholine.

Polarized IR of TM Peptides with V-ATPase Inhibitors. Experiments were carried out with the classical V-ATPase inhibitor, concanamycin A, and with the most potent from the family of synthetic 5-(2-indolyl)-2,4-pentadienoyl inhibitors, INDOL0, at a 1:1 mole ratio with respect to the TM peptide. Table 7 gives the order parameters and effective tilts of the α-helices and the lipid chains for Vma3p TM4 and Vph1p TM7, in fluid hydrated DOPC membranes, with and without added inhibitor. Equimolar indolyl inhibitor, INDOL0, has little effect on the orientation of the Vph1p TM7 peptide, either at 10 °C or at 36 °C, but decreases the order of the Vma3p TM4 peptide. Concanamycin A, however, causes an increase in the order of the two TM peptides, indicating an interaction of the inhibitor with both. Infrared absorption by INDOL0 in the amide I region prevents the use of higher inhibitor/peptide ratios that might be required to express effects equivalent to those induced by equimolar concanamycin A.

Secondary Structure of TM Peptides in Lipid Membranes. Band fitting (see, e.g., Figure 9) was performed for the absorption spectra in the amide I region, recorded with parallel and perpendicularly polarized radiation, to determine the relative contents of the different secondary structural elements. To obtain the true intensities from the aligned samples, the absorbances of the individual components in parallel and perpendicular polarization were combined according to eq 3. Initial experiments indicated that hydrated membrane samples prepared from Vma3p TM peptides dissolved in trifluoroethanol (TFE) contained a high proportion of β-sheet structure, with the most prominent peak at 1625 cm^{-1}, particularly at relatively low lipid/protein ratios. Therefore, all subsequent experiments were performed on samples prepared from peptides dissolved in hexafluoroisopropanol (HFIP). Peptide Vma3p TM3 was found by ATR to be in a β-sheet configuration in all mixtures with dried and subsequently hydrated lipids. Presumably, this is because the peptide cannot incorporate in the lipid, resulting in extensive aggregation in the initially dry state. That the Vma3p TM3 peptide does not incorporate in the hydrophobic environment of phospholipids is consistent with thermodynamic predictions in Table 3 and with the inward-facing orientation of this transmembrane segment, not exposed to lipid, in subunit *c* assemblies (cf. Figure 1 and ref *14*). No lipid-peptide interaction with Vma3p TM3 was detected by

Table 7: Order Parameters, $\langle P_2(\cos\gamma)\rangle$, and Effective Tilts, γ_{eff} (°), of the α-Helices (Amide I) of TM Peptides and of the Lipid Chains (CH_2) in Aligned Hydrated DOPC multibilayers, at the Temperatures Indicated, In the Presence and Absence of Inhibitors at a 1:1 mol/mol Ratio with Respect to Peptide[a]

inhibitor	lipid/peptide (mol/mol)	CH_2		amide I	
		10 °C	36 °C	10 °C	36 °C
		Vph1p TM7			
—	20:1	0.28 (44°)	0.25 (45°)	−0.25 (66°)	−0.14 (61°)
INDOL0	20:1	0.31 (43°)	0.26 (44°)	−0.24 (66°)	−0.17 (62°)
concanamycin	20:1	0.19 (47°)	0.13 (49°)	−0.17 (62°)	−0.07 (57°)
		Vma3p TM4			
—	20:1	0.27 (44°)	0.27 (44°)	−0.09 (59°)	−0.01 (55°)
INDOL0	20:1	0.27 (44°)	0.21 (46°)	−0.20 (63°)	−0.12 (60°)
—	12:1	0.31 (43°)	0.27 (44°)	−0.30 (68°)	−0.18 (63°)
concanamycin	12:1	0.27 (44°)	0.25 (45°)	−0.21 (64°)	−0.09 (59°)

[a] Order parameters and effective tilts (given in parentheses) are obtained from eqs 1 and 2, respectively.

Table 8: Results of Band Fitting of the Amide I Region in the Polarized ATR Spectra of Vma3p TM4, Vma3p TM2, and Vph1p TM7 Peptides in Aligned Hydrated Lipid Multibilayers, at the Lipid/Peptide Molar Ratios Indicated[a]

peptide	lipid/peptide (mol/mol)	helix content (%)		β sheet content (%)	
		10 °C	36 °C[b]	10 °C	36 °C[b]
Vma3p TM4	DOPC 90:1	81	78	19	22
	DOPC 50:1	84	81	16	19
	DOPC 20:1	69	67	29	32
	DOPC 12:1	69	68	30	31
	DMPC 50:1	75	74	25	26
	DPPC 50:1	78	80	22	19
	DMPG 50:1	78	79	22	21
	DOPG 50:1	80	81	20	19
Vph1p TM7	DOPC 50:1	85	90	13	7
	DOPC 20:1	58	59	37	37
	DOPC 12:1	55	55	36	35
	DPPC 50:1	57	59	37	37
Vma3p TM2	DOPC 20:1	57	55	26	30
	DOPC 12:1	48	52	26	27

[a] Net intensities of the component bands are determined from absorbances with parallel and perpendicular polarized radiation according to eq 3 (*31*). [b] For DPPC, 45 °C.

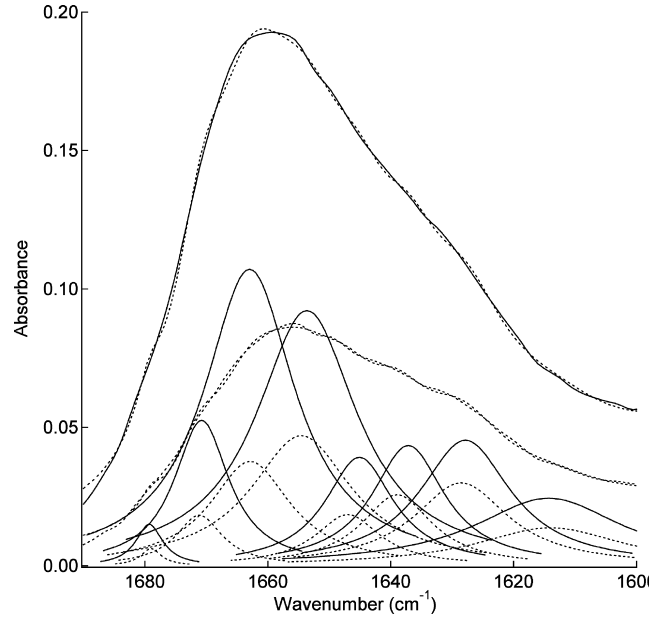

FIGURE 10: Amide I region in the polarized ATR infrared spectra from aligned 16-kDa proteolipid membranes from *Nephrops norvegicus* in D_2O buffer, at a temperature of 36 °C. Solid lines are for parallel-polarized (0°) radiation; dotted lines are for perpendicular-polarized (90°) radiation. Band fitting is shown below the experimental spectra, and the fitted envelope is given by dotted lines. The component at lowest frequency is not included in quantifying the amide I band.

spin-label EPR (data not shown), again consistent with total lack of membrane incorporation of this peptide.

Analysis of the secondary structure was performed for the three different peptides, Vma3p TM4, Vma3p TM2, and Vph1p TM7, in a variety of different lipids and over a range of lipid/peptide ratios. Results from quantitation of the band fitting are presented in Table 8. For fluid membranes, the Vma3p TM4 peptide is highly α-helical in most lipids tested and over a wide range of lipid/peptide ratio in DOPC (cf. also Figures 8 and 9). A minor spectral component at low frequency, corresponding to β-sheet, appears most appreciably for low lipid/peptide ratios (20:1 and 12:1 mol/mol) in DOPC. For the Vph1p TM7 peptide, the situation is somewhat similar but with a more pronounced dependence on lipid/peptide ratio in DOPC. The major α-helical band has an asymmetrical shoulder at 1630 cm^{-1} for a lipid/peptide ratio of 20:1 mol/mol in DOPC (see Figure 8). This lack of resolution hampers the quantitation, and it may be that the β-sheet contents given in Table 8 are overestimates. For the Vma3p TM2 peptide, the spectrum at 20:1 mol/mol in DOPC contains a major peak at the α-helical frequency of ca. 1655 cm^{-1} but also a resolved peak at the β-sheet frequency of ca. 1622 cm^{-1} (see Figure 8). At a lipid/peptide ratio of 12:1 mol/mol, the situation for Vma3p TM2 is rather similar to that at 20:1 mol/mol.

Polarized IR of Nephrops 16-kDa Proteolipid Membranes. The 16-kDa proteolipid from *Nephrops norvegicus* can substitute functionally for V-ATPase subunit *c* in *S. cerevisiae* (*45*). Membranous hexameric assemblies of the *Nephrops* protein, therefore, provide a useful comparison with the behavior of the synthetic Vma3p peptides (*17, 39*).

Figure 10 shows the amide I region from polarized ATR infrared spectra of aligned 16-kDa proteolipid membranes in D_2O buffer. Infrared transmission spectra from random dispersions of such membranes have been reported previously (*45*). The spectra are characterized by the major peak at higher frequency, in the α-helix region, with a lower-intensity flank on the low-frequency side. As found previously (*45*), band fitting reveals two bands in the α-helical region: one closer to the conventional frequency of ca. 1656 cm^{-1} and the other at a higher frequency of ca. 1664 cm^{-1}. The latter

component is found also in the infrared spectrum of bacteriorhodopsin (*46*), which is overwhelmingly α-helical (*47*). Quantitation of the relative populations by band fitting (and using eq 3) yields an α-helical content of ca. 56%, in reasonable agreement with previous findings on random membrane dispersions (*45*).

The α-helical bands of the 16-kDa proteolipid display a pronounced dichroism. The order parameters and effective tilt angles for the total α-helical component were calculated in exactly the same way as for the TM peptides. The average helix order parameter is $\langle P_2(\cos\gamma)\rangle = 0.20 \pm 0.01$, at both 10 and 36 °C. This corresponds to an effective tilt (from eq 2) of $\gamma_{eff} \approx 47°$. These values are unchanged by the addition of concanamycin A at a ratio of 7:1 mol/mol, relative to the 16-kDa monomer. Membranes were centrifuged and resuspended in D_2O buffer in order to remove the DMSO in which concanamycin A was added.

It is notable that the helices in the putative 4-helix bundles of the 16-kDa proteolipid are considerably more ordered than are the Vma3p TM4 and Vph1p TM7 peptides alone in lipid membranes but have a mean effective tilt similar to that of Vma3p TM2 (cf. Tables 4–7). It is also of interest that the helices of the two Vma3p TM peptides have amide I bands at the normal frequency for α-helices, without any component at the higher frequency of ca. 1664 cm^{-1} that is present in the 16-kDa proteolipid membranes (compare, for example, Figures 9 and 10).

DISCUSSION

Spontaneous self-assembly of the Vma3p TM4, Vma3p TM2, and Vph1p TM7 peptides in lipid membranes is demonstrated here via the effect on the lipid–protein interactions. IR spectroscopy demonstrates that, under these conditions of oligomer formation, the peptides are in a predominantly α-helical conformation. This is also true for the equimolar combination of Vma3p TM4 and Vph1p TM7 peptides. In the latter case, interaction between the complementary rotor-stator pair is evidenced by changes both in the lipid–protein interactions and in the orientation of the peptide helices. Direct contact between Vph1p TM7 and Vma11p TM4 (of subunit *c′*) in the intact V-ATPase has been demonstrated previously by disulphide cross-linking (*48*) but not so far with Vma3p TM4 (of subunit *c*).

Lipid Stoichiometry and Peptide Assembly. Oligomeric sizes of the peptide assemblies can be estimated from the stoichiometry of lipid−peptide interaction, N_b, per monomer that is obtained from measurements with 14-PCSL in the DOPC host matrix. The larger the oligomer, the greater is the extent of peptide–peptide contact, and consequently, the interfacial contact between lipid and peptide monomers is reduced on increasing the size of the oligomer. For a helical sandwich (or regular polygonal arrangement) that is composed of n_α α-helices, the stoichiometry of first-shell lipids surrounding the peptide assembly is given by (*42, 49*) the following equation:

$$N_b \times n_\alpha = \pi(D_\alpha/d_{ch} + 1) + n_\alpha D_\alpha/d_{ch} \quad (4)$$

where N_b is the number of motionally restricted lipids per helix (i.e., per peptide), d_{ch} (≈0.48 nm) is the diameter of a lipid chain, and D_α (≈1.0 nm) is that of an α-helix. This would predict that $n_\alpha \approx 6$ for the Vma3p TM4 assemblies ($N_b = 3.7$ per monomer), which could correspond to a very limited association of 4-helix bundles. A similar calculation yields a higher degree of association: $n_\alpha \approx 14$ for the Vph1p TM7 assemblies, corresponding to the lower stoichiometry of motionally restricted lipid ($N_b \sim 2.8$ per monomer). In the case of a polygonal arrangement, these values correspond to the outer ring of TM helices, facing the lipid (cf. Figure 1). If it is assumed that the ring is composed of 4-helix bundles, each contributing 2 helices to the outer rim, as in the NtpK structure (*14*), then the effective number of 16-kDa proteolipid tetrameric subunits is half the above values of n_α, that is, trimers and heptamers for putative Vma3p TM4 and Vph1p TM7 homotetramer subunits, respectively. If the inner rim of the ring is also accessible to lipid (as in the NtpK structure), these numbers are decreased by a further factor of 2.

The equimolar mixture of Vma3p TM4 with Vph1p TM7 restricts fewer lipids per helix than do either of the two TM peptides alone. This implies that Vma3p TM4 and Vph1p TM7 coassemble into structures that are larger than the homo-oligomers of either peptide alone. When the stoichiometry of motionally restricted lipids approaches $N_b \sim 2$, oligomer sizes cannot be determined precisely from eq 4. Nonetheless, a minimum size of $n_\alpha > 30$ helices per oligomer can be estimated for the coassembled Vma3p TM4 and Vph1p TM7 peptides, i.e., values which approach the size of the V_o assemblies in V-ATPases. This enhanced degree of association, relative to the single peptides alone, may be attributed, at least in part, to the formation of salt bridges between Arg^{735} of Vph1p TM7 and Glu^{137} of Vma3p TM4, as envisaged in the rotary mechanism of proton transport. Alone, the glutamate of Vma3p TM4 would be protonated when in the hydrophobic interior of the membrane, but no such energetically favorable neutralization is possible for the unique arginine residue of Vph1p TM7. The energetic penalty of burying Arg^{735} of this longer peptide in the lipid membrane is offset by introducing more apolar residues into the membrane than are included in the shorter peptides (see Figure 4 and Table 3). As already noted, direct interaction of the Vph1p TM7 peptide with Vma3p TM4 is indicated by the increase in its ordering on coassembly.

Helix Packing Motifs. A recent survey of the three-dimensional structures of integral proteins indicates that transmembrane α-helices tend to pack with well-defined crossing angles (*50*). The major populations either have the Ala-coil packing mode that is characterized by small residues seven apart (*a* and *g*), with small residues also at the fourth or fifth positions (*d* or *e*), or are analogues of the classical GX_3G motif with small residues four apart. The former group has relatively small crossing angles, whereas the latter has crossing angles in the region of 40°.

The Vma3p TM4 peptide is devoid of the Ala-coil heptad motif, but Vma3p TM2 has two heptad repeats (*a*, *g*), one of which has a small residue also at the fifth position (*e*) ($S^{71}X_3A^{75}XS^{77}$). The Vph1p TM7 peptide contains three heptads, only one of which has a small residue at the intermediate *d*- or *e*-position ($A^{738}X_3A^{742}XA^{744}$). All three peptides are relatively rich in analogues of the GX_3G motif: three in Vma3p TM2 ($A^{60}X_3A^{64}$, $G^{67}X_3S^{71}$, and $S^{71}X_3A^{75}$), two in Vma3p TM4 ($A^{136}X_3G^{140}$ and $G^{143}X_3A^{147}$), and three in Vph1p TM7 ($S^{728}X_3S^{732}$, $A^{738}X_3A^{742}$, and $A^{744}X_3S^{748}$). Thus, the peptides derived from subunits *a* and *c* of the V_o-

sector of *S. cerevisiae* V-ATPase contain helix packing motifs that would allow their self-assembly into homo-oligomers with either parallel or antiparallel orientations, consistent with our observations. In addition, the packing motifs in Vma3p TM4 and Vph1p TM7 are adequate to allow coassembly of these two peptides, as indicated by the results with spin-labeled lipids.

Peptide Tilts. The axes of all peptide helices exhibit large angular deviations from the substrate normal. Alone, the crossing angles of the helices are insufficient to account for these large tilts. For the packing of two helices according to the GX_3G motif, the tilt angle would be in the region of 20°, if the axis of symmetry were parallel to the membrane normal. The observed tilts, therefore, imply that the symmetry axes of the helix pairs within a bundle deviate from the membrane normal.

One reason that the peptides may tilt is to match their hydrophobic span with that of the hydrocarbon core of the lipid bilayer (*51–53*). For complete matching between peptide and lipid, the inclination, γ, of the peptide to the bilayer normal is given by

$$\cos\gamma = \frac{d_c(\text{nm})}{0.15 \times N_{res}} \quad (5)$$

where d_c is the hydrocarbon thickness of the bilayer, and N_{res} is the number of residues in the hydrophobic span of the peptide. An α-helical repeat distance of 0.15 nm is assumed. The hydrophobic thickness of DOPC bilayers at 36 °C is $d_c = 2.63$ nm, corrected from the most recent high-resolution X-ray measurements (*54*) with an expansion coefficient of -0.0033 K^{-1} (*55, 56*). From Table 1, the hydrophobic spans of the Vma3p TM2 and TM4 peptides are $N_{res} = 21$ and 26, respectively, and that of the Vph1p TM7 peptide can be taken as minimally $N_{res} = 30$ from Figure 2. With these values, eq 5 predicts tilt angles of $\gamma =$ 26°, 48°, and 54° for Vma3p TM2, Vma3p TM4, and Vph1p TM7, respectively.

Comparing with Table 4, one sees that the predicted tilts are in the relative order measured experimentally but are significantly smaller. Taking the full length of the three peptides yields values of $\gamma = 46°$, 51°, and 62°, which are similar to the experimental measurements but are likely to be an overestimate. Added to this, measurements with model transmembrane peptides (*57, 58*) and of lipid association constants with integral proteins indicate that a degree of hydrophobic mismatch can be tolerated (*59*). The effects of mismatch additionally will be reduced by the tendency of the Vma3p and Vph1p helices to self-associate, as is demonstrated by the results with spin-labeled lipids. Similar calculations for Vma3p TM4 in fluid DMPC and DPPC bilayers, using comparable high-resolution X-ray data (*55, 60*), predict tilts for complete hydrophobic matching that are comparable in size to the experimental values in Table 6 but which again are somewhat smaller.

The 16-kDa proteolipid from *Nephrops* contains the TM1 and TM3 helices, which likely face inward, away from the lipid, in addition to helices TM2 and TM4, which face outward, toward the lipid (see Figure 1 and ref *14*). Nonetheless, the average tilt is comparable to that of Vma3p TM2 but less than that of Vma3p TM4 (cf. Table 4). In terms of hydrophobic matching, this is consistent with the finding that cholesterol-containing lipid bilayers, such as those of 16-kDa proteolipid membranes (*17*), have a larger hydrophobic thickness than those without cholesterol (*61–64*).

Recently, it has been suggested that the effective tilt of proteins in membranes aligned on orienting substrates (as in infrared dichroism measurements) is augmented by inclinations of the local director, which arise from elastic bending fluctuations of the membrane (*65*). In the case of low lipid/peptide ratios, these would correspond instead to a local static curvature. Thus, whereas a substantial proportion of the tilt of the Vma3p and Vph1p peptides can be ascribed to hydrophobic matching, other mechanisms will contribute in addition (see also above). Coassembly of the Vma3p TM4 and Vph1p TM7 peptides may give rise to a mode of helix packing that differs from that of the homo-oligomers and which results in different tilt angles (cf. Tables 4 and 7). This points to a further factor that affects the net tilt of the peptide helices.

CONCLUSIONS

The Vma3p peptides of subunit *c* that are thought to face the lipid in the intact V-ATPase (TM2 and TM4; see Figure 1) and the corresponding Vph1p peptide of subunit *a* (TM7) incorporate in lipid bilayers, consistent with thermodynamic predictions (see Table 3), and self-assemble into membrane-spanning helical bundles. In addition, the complementary rotor and stator peptides, Vma3p TM4 and Vph1p TM7, which are predicted to form the proton translocation pathway, coassemble in lipid membranes. Thus, these peptides contain packing motifs that may represent functional assembly of the V_o-sector in the intact V-ATPase, and their behavior in lipid bilayers could reproduce some of the native interactions.

The classical V-ATPase inhibitor concanamycin interacts both with Vma3p TM4 from the rotor assembly and with Vph1p TM7 from the stator assembly, whereas direct evidence for interaction of the indolyl inhibitor INDOL0 is obtained only with Vma3p TM4 (see Table 7). This possibly may be connected with the selectivity of INDOL0 for the osteoclast V-ATPase (*7, 8*) because discriminatory properties of this type of small-molecule inhibitor have been attributed to the presence of tissue-specific subunit *a* isoforms. It seems likely, however, that the inhibitory activity of both compounds may involve disrupting the interaction between this complementary pair of transmembrane helices in the rotary mechanism of proton translocation (cf. Figure 1). Although the majority of residues implicated in binding bafilomycin/concanamycin map onto the TM2−TM4 intermolecular junction in Vma3p (*4*), a direct involvement of Vph1p in bafilomycin binding has also been proposed (*66*).

In contrast, interaction of concanamycin with the 16-kDa proteolipid subunit *c* assemblies in *Nephrops* membranes is not detected when using similar methods. This is possibly a dilution effect by the other TM segments, relative to reconstituted membranes containing the single Vma3p TM4 peptide at high concentration. Also, the covalent linkages within the 4-helix bundles of the 16-kDa proteolipid may stabilize these assemblies, making the helix orientation less sensitive to interaction with concanamycin. Potentially, this may be one advantage, additional to the positional selectivity, in favor of using peptides representing the individual TM sequences for such studies.

ACKNOWLEDGMENT

We thank Frau B. Angerstein for the synthesis of spin-labeled lipids and Frau B. Freyberg for skillful technical assistance.

REFERENCES

1. Kawasaki-Nishi, S., Nishi, T., and Forgac, M. (2003) Proton translocation driven by ATP hydrolysis in V-ATPases. *FEBS Lett. 545*, 76–85.
2. Forgac, M. (2007) Vacuolar ATPases: rotary proton pumps in physiology and pathophysiology. *Nature Rev. Mol. Cell Biol. 8*, 917–929.
3. Crider, B. P., Xie, X. S., and Stone, D. K. (1994) Bafilomycin inhibits proton flow through the H^+ channel of vacuolar proton pumps. *J. Biol. Chem. 269*, 17379–17381.
4. Bowman, B. J., and Bowman, E. J. (2002) Mutations in subunit *c* of the vacuolar ATPase confer resistance to bafilomycin and identify a conserved antibiotic binding site. *J. Biol. Chem. 277*, 3965–3972.
5. Huss, M., Ingenhorst, G., König, S., Gassel, M., Dröse, S., Zeeck, A., Altendorf, K., and Wieczorek, H. (2002) Concanamycin A, the specific inhibitor of V-ATPases, binds to the V_o subunit *c*. *J. Biol. Chem. 277*, 40544–40548.
6. Páli, T., Whyteside, G., Dixon, N., Kee, T. P., Ball, S., Harrison, M. A., Findlay, J. B. C., Finbow, M. E., and Marsh, D. (2004) Interaction of inhibitors of the vacuolar H^+-ATPase with the transmembrane V_o-sector. *Biochemistry 43*, 12297–12305.
7. Gagliardi, S., Nadler, G., Consolandi, E., Parini, C., Morvan, M., Legave, M. N., Belfiore, P., Zocchetti, A., Clarke, G. D., James, I., Nambi, P., Gowen, M., and Farina, C. (1998) 5-(5,6-dichloro-2-indolyl)-2-methoxy-2,4-pentadienamides: novel and selective inhibitors of the vacuolar H^+-ATPase of osteoclasts with bone antiresorptive activity. *J. Med. Chem. 41*, 1568–1573.
8. Dixon, N., Páli, T., Kee, T. P., Ball, S., Harrison, M. A., Findlay, J. B. C., Nyman, J., Väänänen, H. K., Finbow, M. E., and Marsh, D. (2008) Interaction of spin-labelled inhibitors of the vacuolar H^+-ATPase with the transmembrane V_0-sector, *Biophys. J.*, *94,* 506–514.
9. Hirata, T., Iwamoto-Kihara, A., Sun-Wada, G. H., Okajima, T., Wada, Y., and Futai, M. (2003) Subunit rotation of vacuolar-type proton pumping ATPase. Relative rotation of the G and c subunits. *J. Biol. Chem. 278*, 23714–23719.
10. Sun-Wada, G. H., Wada, Y., and Futai, M. (2003) Vacuolar H^+ pumping ATPases in luminal acidic organelles and extracellular compartments: common rotational mechanism and diverse physiological roles. *J. Bioenerg. Biomembr. 35*, 347–358.
11. Noumi, T., Beltran, C., Nelson, H., and Nelson, N. (1991) Mutational analysis of yeast vacuolar H^+-ATPase. *Proc. Natl. Acad. Sci. U.S.A. 88,* 1938–1942.
12. Hirata, R., Graham, L. A., Takatsuki, A., Stevens, T. H., and Anraku, Y. (1997) VMA11 and VMA16 encode second and third proteolipid subunits of the *Saccharomyces cerevisiae* vacuolar membrane H^+-ATPase. *J. Biol. Chem. 272*, 4795–4803.
13. Kawasaki-Nishi, S., Nishi, T., and Forgac, M. (2001) Arg-735 of the 100-kDa subunit a of the yeast V-ATPase is essential for proton translocation. *Proc. Natl. Acad. Sci. U.S.A. 98*, 12397–12402.
14. Murata, T., Yamato, I., Kakinuma, Y., Leslie, A. G. W., and Walker, J. E. (2005) Structure of the rotor of the V-type Na^+-ATPase from *Enterococcus hirae*. *Science 308*, 654–659.
15. Arai, H., Terres, G., Pink, S., and Forgac, M. (1988) Topography and subunit stoichiometry of the coated vesicle proton pump. *J. Biol. Chem. 263*, 8796–8802.
16. Wang, Y., Cipriano, D. J., and Forgac, M. (2007) Arrangement of subunits in the proteolipid ring of the V-ATPase. *J. Biol. Chem. 282*, 34058–34065.
17. Páli, T., Finbow, M. E., Holzenburg, A., Findlay, J. B. C., and Marsh, D. (1995) Lipid-protein interactions and assembly of the 16-kDa channel polypeptide from *Nephrops norvegicus*. Studies with spin-label electron spin resonance spectroscopy and electron microscopy. *Biochemistry 34*, 9211–9218.
18. Marsh, D. (1993) The Nature of the Lipid-Protein Interface and the Influence of Protein Structure on Protein-Lipid Interactions, in *New Comprehensive Biochemistry, Vol. 25, Protein-Lipid Interactions* (Watts, A., Ed.) pp 41–66, Elsevier, Amsterdam.
19. Marsh, D., and Horváth, L. I. (1998) Structure, dynamics and composition of the lipid-protein interface. Perspectives from spin-labelling. *Biochim. Biophys. Acta 1376*, 267–296.
20. Páli, T., Bashtovyy, D., and Marsh, D. (2006) Stoichiometry of lipid interaction with transmembrane proteins, deduced from the 3-D structures. *Protein Sci. 15*, 1153–1161.
21. Marsh, D. (1999) Spin label ESR spectroscopy and FTIR spectroscopy for structural/dynamic measurements on ion channels. *Methods Enzymol. 294*, 59–92.
22. Nadler, G., Morvan, M., Delimoge, I., Belfiore, P., Zocchetti, A., James, I., Zembryki, D., Lee-Rycakzewski, E., Parini, C., Consolandi, E., Gagliardi, S., and Farina, C. (1998) (2*Z*,4*E*)- 5(5,6-dichloro-2-indolyl)-2-methoxy-*N*-(1,2,2,6,6-pentamethylpiperidin-4-yl)-2,4-pentadienamide, a novel, potent and selective inhibitor of the osteoclast V-ATPase. *Bioorg. Med. Chem. Lett. 8*, 3621–3626.
23. Hubbell, W. L., and McConnell, H. M. (1971) Molecular motion in spin-labelled phospholipids and membranes. *J. Am. Chem. Soc. 93*, 314–326.
24. Marsh, D. and Watts, A. (1982) Spin-Labeling and Lipid-Protein Interactions in Membranes, in *Lipid-Protein Interactions, Vol. 2* (Jost, P. C., and Griffith, O. H., Eds.) pp 53–126, Wiley-Interscience, New York.
25. Finbow, M. E., Buultjens, T. E. J., Lane, N. J., Shuttleworth, J., and Pitts, J. D. (1984) Isolation and characterisation of arthropod gap junctions. *EMBO J. 3*, 2271–2278.
26. Finbow, M. E., Eliopoulos, E. E., Jackson, P. J., Keen, J. N., Meagher, L., Thompson, P., Jones, P. C., and Findlay, J. B. C. (1992) Structure of 16 kDa integral membrane protein that has identity to the putative proton channel of the vacuolar H^+-ATPase. *Protein Eng. 5*, 7–15.
27. Buultjens, T. E. J., Finbow, M. E., Lane, N. J., and Pitts, J. D. (1988) Tissue and species conservation of the vertebrate and arthropod forms of the low molecular weight (16–18000) proteins of gap junctions. *Cell Tissue Res. 251*, 571–580.
28. Marsh, D. (1982) Electron Spin Resonance: Spin Label Probes, in *Techniques in Lipid and Membrane Biochemistry, Vol. B4/II* (Metcalfe, J. C., and Hesketh, T. R., Eds.) pp B426/1–B426/44, Elsevier, Amsterdam.
29. Marsh, D., Müller, M., and Schmitt, F.-J. (2000) Orientation of the infrared transition moments for an α-helix. *Biophys. J. 78*, 2499–2510.
30. Marsh, D., and Páli, T. (2001) Infrared dichroism from the x-ray structure of bacteriorhodopsin. *Biophys. J. 80*, 305–312.
31. Marsh, D. (1999) Quantitation of secondary structure in ATR infrared spectroscopy. *Biophys. J. 77*, 2630–2637.
32. White, S. H., and Wimley, W. C. (1998) Hydrophobic interactions of peptides with membrane interfaces. *Biochim. Biophys. Acta 1376*, 339–352.
33. Jayasinghe, S., Hristova, K., and White, S. H. (2001) Energetics, stability, and prediction of transmembrane helices. *J. Mol. Biol. 312*, 927–934.
34. Eisenberg, D., Schwarz, E., Komaromy, M., and Wall, R. (1984) Analysis of membrane and surface protein sequences with the hydrophobic moment plot. *J. Mol. Biol. 179*, 125–142.
35. Wu, C. H., Yeh, L.-S. L., Huang, H., Arminski, L., Castro-Alvear, J., Chen, Y., Hu, Z., Kourtesis, P., Ledley, R. S., Suzek, B. E., Vinayaka, C. R., Zhang, J., and Barker, W. C. (2003) The protein information resource. *Nucleic Acids Res. 31*, 345–347.
36. Su, Y., Zhou, A., Al-Lamki, R. S., and Karett, F. E. (2003) The a-subunit of the V-type H^+-ATPase interacts with phosphofructokinase-1 in humans. *J. Biol. Chem. 278*, 20013–20018.
37. Leng, X.-H., Nishi, T., and Forgac, M. (1999) Transmembrane topography of the 100-kDa a subunit (vph1p) of the yeast vacuolar proton-translocating ATPase. *J. Biol. Chem. 274*, 14655–14661.
38. Harrison, M. A., Murray, J., Powell, B., Kim, Y. I., Finbow, M. E., and Findlay, J. B. C. (1999) Helical interactions and membrane disposition of the 16-kDa proteolipid subunit of the vacuolar H^+-ATPase analyzed by cysteine replacement mutagenesis. *J. Biol. Chem. 274*, 25461–25470.
39. Páli, T., Finbow, M. E., and Marsh, D. (1999) Membrane assembly of the 16-kDa proteolipid channel from *Nephrops norvegicus* studied by relaxation enhancements in spin-label ESR. *Biochemistry 38*, 14311–14319.
40. Harrison, M., Powell, B., Finbow, M. E., and Findlay, J. B. C. (2000) Identification of lipid-accessible sites on the Nephrops 16-kDa proteolipid incorporated into a hybrid vacuolar H^+-ATPase: Site-directed labeling with *N*-(1-pyrenyl)cyclohexylcarbodiimide and fluorescence quenching analysis. *Biochemistry 39*, 7531–7537.

41. Findlay, J. B. C., and Harrison, M. A. (2002) A protein chemical approach to channel structure and function: the proton channel of the vacuolar H^+-ATPase. *Novartis Found. Symp. 245*, 207–218.
42. Marsh, D. (1997) Stoichiometry of lipid-protein interaction and integral membrane protein structure. *Eur. Biophys. J. 26*, 203–208.
43. Marsh, D. (1990) *Handbook of Lipid Bilayers* CRC Press, Boca Raton, FL.
44. Nagle, J. F., and Tristram-Nagle, S. (2000) Structure of lipid bilayers. *Biochim. Biophys. Acta 1469*, 159–195.
45. Holzenburg, A., Jones, P. C., Franklin, T., Páli, T., Heimburg, T., Marsh, D., Findlay, J. B. C., and Finbow, M. E. (1993) Evidence for a common structure for a class of membrane channels. *Eur. J. Biochem. 213*, 21–30.
46. Earnest, T. N., Herzfeld, J., and Rothschild, K. J. (1990) Polarized Fourier transform infrared spectroscopy of bacteriorhodopsin. Transmembrane α helices are resistant to hydrogen/deuterium exchange. *Biophys. J. 58*, 1539–1546.
47. Luecke, H., Schobert, B., Richter, H.-T., Cartailler, J.-P., and Lanyi, J. K. (1999) Structure of bacteriorhodopsin at 1.55 Å resolution. *J. Mol. Biol. 291*, 899–911.
48. Kawasaki-Nishi, S., Nishi, T., and Forgac, M. (2003) Interacting helical surfaces of the transmembrane segments of subunits a and c′ of the yeast V-ATPase defined by disulfide-mediated cross-linking. *J. Biol. Chem. 278*, 41908–41913.
49. Arora, A., Williamson, I. M., Lee, A. G., and Marsh, D. (2003) Lipid-protein interactions with cardiac phospholamban studied by spin-label electron spin resonance. *Biochemistry 42*, 5151–5158.
50. Walters, R. F., and DeGrado, W. F. (2006) Helix-packing motifs in membrane proteins. *Proc. Natl. Acad. Sci. U.S.A. 103*, 13658–13663.
51. Killian, J. A. (1998) Hydrophobic mismatch between proteins and lipids in membranes. *Biochim. Biophys. Acta 1376*, 401–415.
52. Park, S. H., and Opella, S. J. (2005) Tilt angle of a trans-membrane helix is determined by hydrophobic mismatch. *J. Mol. Biol. 350*, 310–318.
53. Ramakrishnan, M., Qu, J., Pocanschi, C. L., Kleinschmidt, J. H., and Marsh, D. (2005) Orientation of β-barrel proteins OmpA and FhuA in lipid membranes. Chainlength dependence from infrared dichroism. *Biochemistry 44*, 3515–3523.
54. Kučerka, N., Tristram-Nagle, S., and Nagle, J. F. (2006) Structure of fully hydrated fluid phase lipid bilayers with monounsaturated chains. *J. Membr. Biol. 208*, 193–202.
55. Kučerka, N., Liu, Y., Chu, N., Petrache, H. I., Tristram-Nagle, S., and Nagle, J. F. (2005) Structure of fully hydrated fluid phase DMPC and DLPC lipid bilayers using x-ray scattering from oriented multilamellar arrays and from unilamellar vesicles. *Biophys. J. 88*, 2626–2637.
56. Marsh, D., Jost, M., Peggion, C., and Toniolo, C. (2007) Lipid chainlength dependence for incorporation of alamethicin in membranes: EPR studies on TOAC-spin labelled analogues. *Biophys. J. 92*, 4002–4011.
57. de Planque, M. R. R., Greathouse, D. V., Koeppe II, R. E., Schäfer, H., Marsh, D., and Killian, J. A. (1998) Influence of lipid/peptide hydrophobic mismatch on the thickness of diacylphosphatidylcholine bilayers. A ^{2}H NMR and ESR study using designed transmembrane α-helical peptides and gramicidin A. *Biochemistry 37*, 9333–9345.
58. de Planque, M. R. R., Kruijtzer, J. A. W., Liskamp, R. M. J., Marsh, D., Greathouse, D. V., Koeppe, II, R. E., De Kruijff, B., and Killian, J. A. (1999) Different membrane anchoring positions of tryptophan and lysine in synthetic transmembrane α-helical peptides. *J. Biol. Chem. 274*, 20839–20846.
59. Marsh, D. (2008) Energetics of hydrophobic matching in lipid-protein interactions, *Biophys. J.* [Online early access], Doi: 10.1529/biophysj.107.121475.
60. Kučerka, N., Tristram-Nagle, S., and Nagle, J. F. (2006) Closer look at structure of fully hydrated fluid phase DPPC bilayers. *Biophys. J. 90*, L83–L85.
61. Lecuyer, H., and Dervichian, D. G. (1969) Structure of aqueous mixtures of lecithin and cholesterol. *J. Mol. Biol. 45*, 39–57.
62. Schreier-Muccillo, S., Marsh, D., Dugas, H., Schneider, H., and Smith, I. C. P. (1973) A spin probe study of the influence of cholesterol on motion and orientation of phospholipids in oriented multibilayers and vesicles. *Chem. Phys. Lipids 10*, 11–27.
63. Marsh, D. (1974) An interacting spin label study of lateral expansion in dipalmitoyl lecithin-cholesterol bilayers. *Biochim. Biophys. Acta 363*, 373–386.
64. McIntosh, T. J. (1978) The effect of cholesterol on the structure of phosphatidylcholine bilayers. *Biochim. Biophys. Acta 513*, 43–58.
65. Marsh, D., Shanmugavadivu, B., and Kleinschmidt, J. H. (2006) Membrane elastic fluctuations and the insertion and tilt of β-barrel proteins. *Biophys. J. 91*, 227–232.
66. Wang, Y., Inoue, T., and Forgac, M. (2005) Subunit a of the yeast V-ATPase participates in binding of bafilomycin. *J. Biol. Chem. 280*, 40481–40488.

BI7025112